ACS OMEGA

Article

Cite This: ACS Omega 2018, 3, 16436−16442

http://pubs.acs.org/journal/acsodf

Immobilizing Ultrafine PtNi Nanoparticles within Graphitic Carbon Nanosheets toward High-Performance Hydrogenation Reaction

Linlin Xu,[†] Jingfei Zhang,[‡] Lin Xu,*[,‡] and Jun Yang*[,†,§]

[†]State Key Laboratory of Multiphase Complex Systems, Institute of Process Engineering, and [§]Center for Mesoscience, Institute of Process Engineering, Chinese Academy of Sciences, Beijing 100190, China

[‡]Jiangsu Key Laboratory of New Power Batteries, Jiangsu Collaborate Innovation Centre of Biomedical Functional Materials, School of Chemistry and Materials Science, Nanjing Normal University, Nanjing 210023, China

Supporting Information

ABSTRACT: Immobilization of Pt-based nanoparticles on carbon support is of great significance in catalysis for their superior activity and enhanced durability. Herein, we report for the first time a feasible NaCl template-engaged approach to firmly immobilize PtNi nanoparticles into two-dimensional (2D) graphitic carbon nanosheets (denoted as PtNi@GCNs hereafter). The elaborate employment of the NaCl template regulates the formation of 2D graphitic carbon nanosheets, which tightly immobilize the in situ-generated PtNi nanoparticles. The smart integration of catalytically active PtNi nanoparticles with carbon nanosheets endows the as-prepared PtNi@GCNs with superior catalytic activity and outstanding stability toward the hydrogenation of 4-nitrophenol, making them a promising catalyst for environmental remediation. We believe that the present work can inspire the future design of carbon nanosheet-based nanohybrids with unique functionalities for diverse applications.

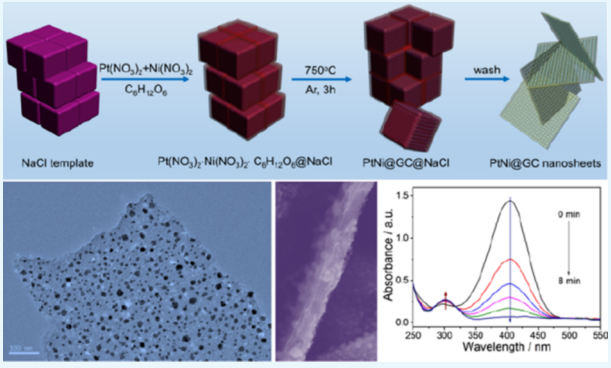

1. INTRODUCTION

Owing to their unique physiochemical properties, noble metal nanoparticles (NPs), especially Pt-based NPs, have demonstrated appealing applications in various realms, including optical devices,[1−3] photocatalysis,[4−7] fuel cell systems,[8−18] and environmental remediation.[19−26] However, in the catalytic field in particular, small-sized metal NPs with relatively high surface energy are prone to aggregate together to form larger particles, resulting in a substantial reduction of the utilization efficiency of noble metal atoms and unsatisfactory stability in practical applications.

One of the effective approaches to suppress the undesirable aggregation of noble metal NPs is to immobilize them on an appropriate substrate, such as carbon-based nanomaterials.[14,27−29] Hybridization with carbon support with high surface area and superior mechanical robustness not only ensures the good dispersion of active metal NPs, but also greatly improves the long-term stability of the catalyst because of the affinity between metal NPs and the carbon support. As a member of the carbon family, two-dimensional (2D) graphitic carbon nanosheets have been documented as a promising candidate because of their cost effectiveness, large surface area, and unique structural anisotropy.[30−33] Nevertheless, previous protocols regarding the immobilization of metal NPs usually involve multistep fabrication procedures and the NPs often easily detach from the support because of the weak binding with the carbon support. In this context, it is highly imperative to develop a feasible and reliable approach to strongly anchor noble metal NPs with 2D graphitic carbon nanosheets, yet it still remains a great challenge. On the other hand, alloying Pt with low-cost transition metals (TMs), such as Fe, Co, Ni, and Cu, to form bimetallic Pt-TM alloys can not only reduce the usage of precious Pt, but also facilitate modifying the electronic structure of Pt, which usually results in better catalytic properties as compared with monometallic counterparts or their physical mixture. Taken together, intimate immobilization of bimetallic Pt-TM NPs into 2D graphitic carbon nanosheets is reasonably anticipated to afford superior catalytic activity and improved stability.

Motivated by the above considerations, we herein for the first time demonstrate a facile NaCl-templated strategy to prepare 2D graphitic carbon nanosheets embedded by PtNi NPs (denoted as PtNi@GCNs). The elaborate employment of the NaCl template regulates the formation of 2D graphitic carbon nanosheets, which firmly immobilize the in situ-generated PtNi NPs. Thanks to the abundant firmly stabilized PtNi NPs for catalytic sites and unique 2D sheetlike structure for electron transport and mass diffusion, the prepared PtNi@GCNs exhibit extraordinary catalytic performance toward the hydrogenation of *p*-nitrophenol (4-NP) with superior activity and stability, as

Received: October 10, 2018
Accepted: November 21, 2018
Published: December 3, 2018

DOI: 10.1021/acsomega.8b02746
ACS Omega 2018, 3, 16436−16442

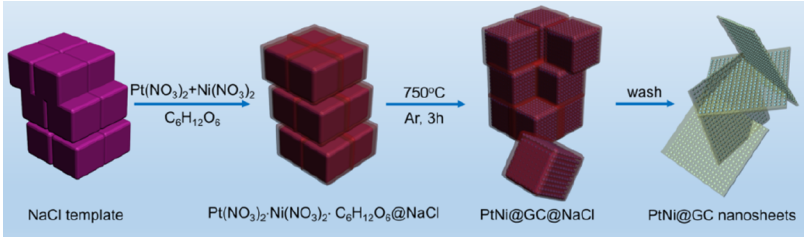

Figure 1. Schematic illustration showing the synthesis of PtNi NP-embedded 2D graphitic carbon nanosheets (PtNi@GCNs) using NaCl as the template.

compared with the commercial Pt/C catalyst. These findings suggest that the as-synthesized PtNi@GCNs may hold grand promise in environmental remediation and electrochemical energy conversion.

2. EXPERIMENTAL SECTION

2.1. Synthesis of the 2D PtNi@GCNs. For the typical synthesis of PtNi@GCNs, 0.2 g of glucose, 0.05 g of $Pt(NO_3)_2$, 0.045 g of $Ni(NO_3)_2{\cdot}6H_2O$, and 0.7 g of NaCl were dissolved in 3 mL of HNO_3 (30%) solution, forming a homogeneous solution. The resultant solution was then dried at 60 °C to evaporate the solvent of H_2O. The obtained mixture was subsequently heated to 750 °C for 3 h under an Ar atmosphere in a tube furnace. Once cooled down, the resulting puffy black powder was finally washed with deionized water and ethanol several times to remove the NaCl template. After drying at 50 °C, the 2D PtNi@GCN product could be obtained.

2.2. Physical characterization. The morphology and size of the product were characterized by scanning electron microscopy (SEM, JEOL JSM-7600F), transmission electron microscopy (TEM, Hitachi H-7650, 120 kV), and high-resolution TEM (HRTEM, JEOL JEM-2010F, 200 kV). The X-ray diffraction (XRD) pattern of the product was recorded on a Rigaku D/max-RC diffractometer with Cu Kα radiation (45 kV and 100 mA). X-ray photoelectron spectroscopy (XPS) was performed on a Thermo VG Scientific ESCALAB 250 spectrometer with an Al Kα radiator. The binding energy has been calibrated by means of the C 1s peak energy of 284.6 eV. Thermogravimetric analysis (TGA) was performed on a Netzsch STA 449C thermal analyzer under an air atmosphere. The Brunauer–Emmett–Teller (BET)-specific surface area was measured by a Micromeritics ASAP 2050 at 77 K.

2.3. Catalytic reduction of 4-NP. For the reduction of 4-NP, $NaBH_4$ was used as a reducing agent and noble metal-based nanomaterials were employed as a catalyst. Typically, 2 mL of 4-NP solution (5×10^{-5} M) and 0.5 mL of freshly prepared aqueous $NaBH_4$ solution (0.1 M) were mixed to form 4-nitrophenolate. Subsequently, 10 μL of the synthesized PtNi@GCN catalyst suspension (1 mg mL^{-1}) was introduced into the above solution to initiate the hydrogenation reaction for the formation of 4-aminophenol (4-AP). The entire reduction progress was monitored by the UV–visible absorption spectra recorded on a Shimadzu UV3600 spectrophotometer at room temperature. For comparison, the commercial Pt/C (20 wt %) was also tested as a catalyst under identical conditions.

3. RESULTS AND DISCUSSION

For the typical preparation of PtNi@GCNs, earth-abundant NaCl crystallites are employed as a removable and recyclable template to modulate the overall morphology of the final product. This strategy has been used to produce carbon nanosheet-supported Ni NPs and porous Pt nanosheets for lithium storage and oxygen reduction reaction, respectively.[34,35] Figure 1 schematically illustrates the overall synthetic procedure of PtNi@GCNs. Briefly, a mixture containing appropriate amounts of glucose, NaCl, $Pt(NO_3)_2$, and $Ni(NO_3)_2$ was first dissolved in a diluted HNO_3 solution to form a homogeneous solution, followed by drying at 60 °C. During the evaporation of H_2O molecules, $Pt(NO_3)_2$, $Ni(NO_3)_2$, and glucose were conformally deposited on the surface of NaCl crystallites because of the low solubility of NaCl. Thereby, the surface of NaCl with high thermal stability provides a 2D platform for the growth of graphitic carbon sheets. Upon the subsequent pyrolysis in an Ar atmosphere at an elevated temperature, the coated glucose would be carbonized into graphitic carbon nanosheets, which could simultaneously reduce metal sources into PtNi NPs distributed within the carbon matrix. Finally, the encased NaCl template could be easily removed by copious washing and freestanding 2D graphitic carbon nanosheets embedded by PtNi NPs could be eventually achieved. It is noteworthy that the NaCl template can be readily recycled through a simple recrystallization process, significantly reducing the synthetic cost.

The morphology of the resulting PtNi@GCN sample was first characterized by SEM and TEM. The panoramic SEM image (Figure 2a) reveals the 2D sheetlike structure of the obtained PtNi@GCN sample. The magnified SEM image (Figure 2b) suggests that the lateral size of the PtNi@GCNs is in the range of 8–16 μm. From the front view of the nanosheet (Figure 2c), one can clearly observe that numerous of PtNi NPs with high uniformity are homogeneously encapsulated in the carbon nanosheet. A cross-sectional observation (Figure 2d) discloses

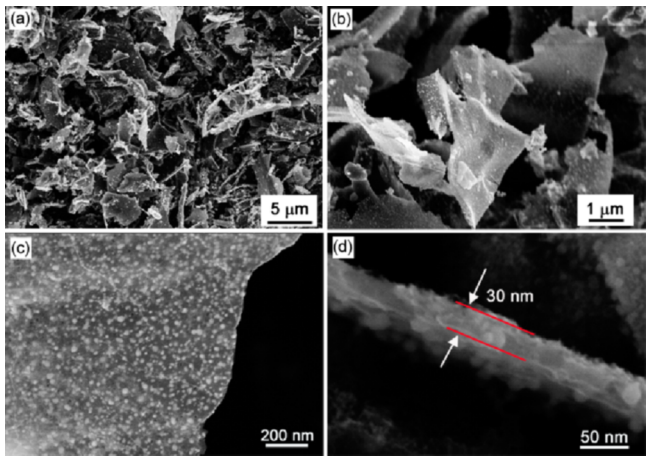

Figure 2. Representative SEM images of the as-synthesized 2D PtNi@GCNs with different magnifications.

DOI: 10.1021/acsomega.8b02746
ACS Omega 2018, 3, 16436–16442

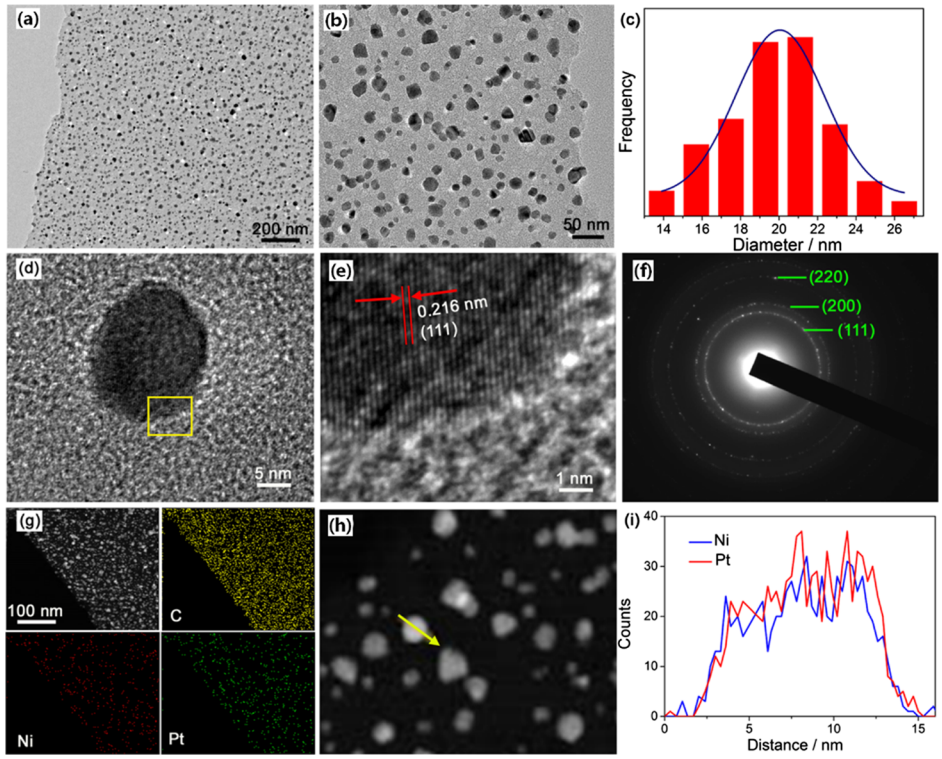

Figure 3. (a,b) TEM images of the as-prepared PtNi@GCNs, (c) histogram showing the particle size distribution of PtNi NPs, (d,e) HRTEM images of an individual PtNi NP, (f) SAED pattern of a PtNi NP, (g) HAADF-STEM image and elemental mappings of the PtNi@GCNs, and (h,i) EDX line-scan profile of a single PtNi NP.

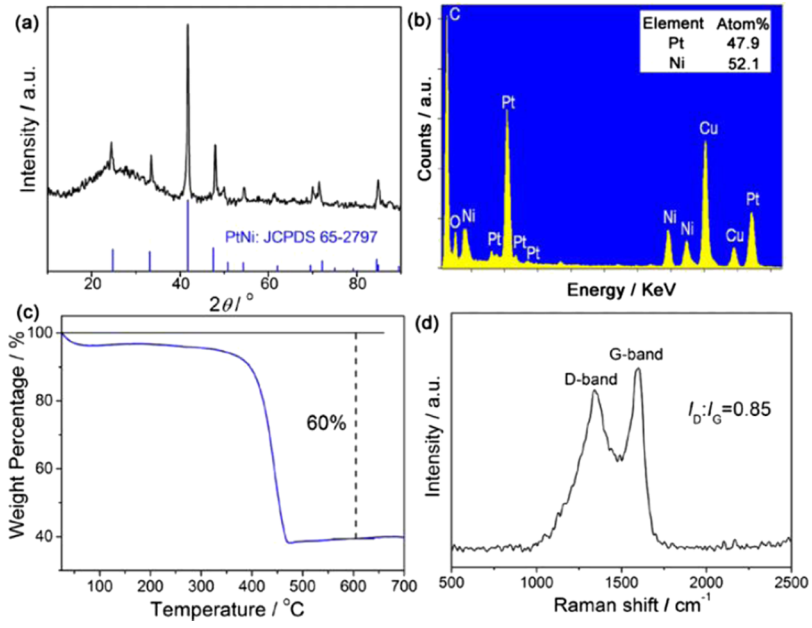

Figure 4. Compositional analyses of the as-prepared 2D PtNi@GCNs: (a) powder XRD pattern, (b) EDX spectrum, (c) TGA curve, and (d) Raman spectrum.

that the thickness of the carbon nanosheet is approximately 30 nm.

In good agreement with the above SEM results, representative TEM images (Figure 3a,b) verify that plenty of well-separated PtNi NPs are discretely dispersed within the carbon matrix, effectively prohibiting the aggregation of the PtNi NPs. A particle size distribution histogram (Figure 3c) of the PtNi NPs indicates that the average diameter of the embedded PtNi NPs is ca. 21 nm. Figure 3d,e presents the HRTEM images of an individual PtNi NP. The well-resolved lattice interplanar spacings are measured to be 0.216 nm, corresponding to the (111) lattice planes of face-centered cubic (fcc)-structured PtNi. The selected area electron diffraction (SAED) pattern suggests the polycrystalline feature of the PtNi NPs and the diffraction rings are assigned to the (111), (200), and (220) planes of fcc-phased PtNi, as marked in Figure 3f. The high-angle annular

DOI: 10.1021/acsomega.8b02746
ACS Omega 2018, 3, 16436−16442

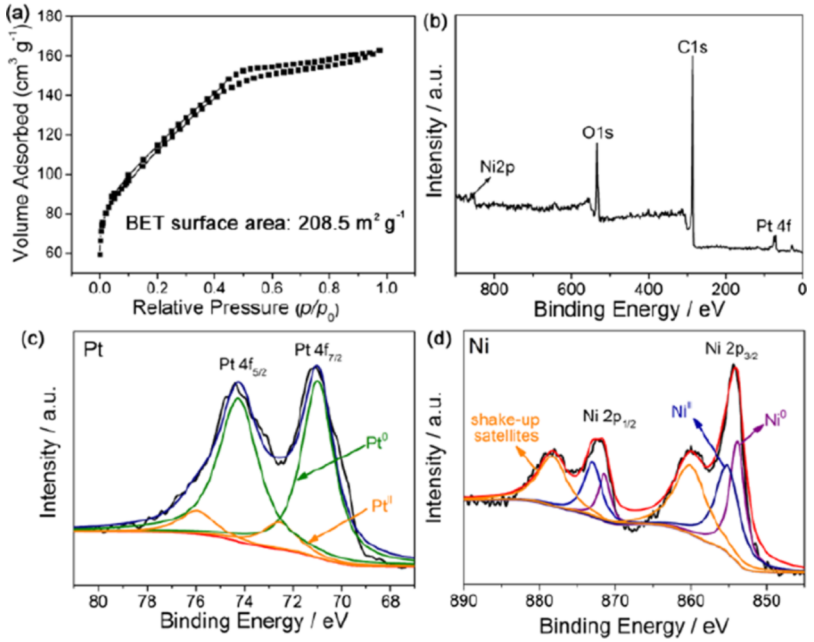

Figure 5. (a) N_2 adsorption−desorption isotherms of the 2D PtNi@GCNs, (b−d) survey scan spectrum, Pt 4f region, and Ni 2p region in the XPS spectra of the 2D PtNi@GCNs, respectively.

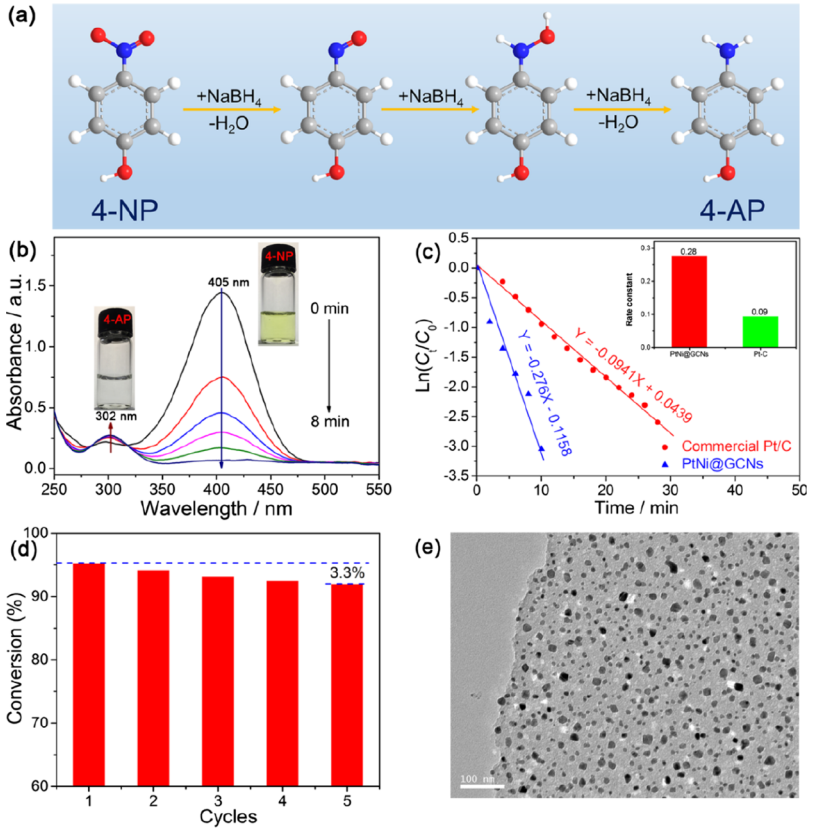

Figure 6. Evaluation of catalytic hydrogenation performance of the PtNi@GCNs: (a) stepwise hydrogenation processes from 4-NP to 4-AP, (b) UV−vis absorption spectra of 4-NP during the hydrogenation reaction catalyzed by PtNi@GCNs, (c) relationships of $\ln(C_t/C_0)$ vs reaction time plot in the presence of different catalysts, (d) recycling tests of hydrogenation of 4-NP over five cycles by using PtNi@GCNs as catalyst, and (e) TEM image of PtNi@GCNs after the recycling tests.

dark-field scanning TEM (HAADF-STEM) and elemental mapping analyses (Figure 3g) imply the uniform distribution of Pt and Ni throughout the entire carbon nanosheets. The cross-sectional compositional line profile (Figure 3i) recorded from an individual PtNi NP (Figure 3h) validates the formation of the PtNi alloy.

The composition of the obtained PtNi@GCN sample was further investigated by the XRD pattern. As shown in Figure 4a,

DOI: 10.1021/acsomega.8b02746
ACS Omega 2018, 3, 16436−16442

the broad peak positioned at ca. 26° is indexed to the (002) plane of graphitic carbon and the other strong diffraction peaks can be well assigned to the PtNi intermetallic alloy (JCPDS no. 65-2797). The energy-dispersive X-ray spectrum shown in Figure 4b confirms the presence of Pt and Ni in the PtNi@GCN product with an atomic ratio of Pt/Ni of around 48/52. The weight percentage of PtNi NPs in the PtNi@GCN nanohybrid was quantified by TGA, as displayed in Figure 4c. The obvious weight loss occurring in the range of 350−450 °C is attributed to the removal of carbon. On the basis of the TGA curve, the weight fraction of PtNi moiety is determined to be 40%. Raman spectroscopy (Figure 4d) is used to evaluate the graphitization degree of the carbon nanosheets. Two distinguished peaks at 1363 and 1596 cm^{-1} are corresponding to the D band and G band of carbon materials, respectively. The relative intensity ratio of the D band to the G band (I_D/I_G) of the PtNi@GCN sample is identified as 0.85, indicating the highly graphitic feature of the carbon nanosheets.

Figure 5a presents the N_2 sorption isotherms of the formed PtNi@GCNs, which can be classified as type-IV isotherms with a noticeable hysteresis loop and suggest the presence of mesopores. Additionally, the steep N_2 uptake at a low relative pressure region implies the presence of micropores, which originate from the gas generated during the decomposition of metal sources at a high temperature. Noticeably, the coexistence of micropores and mesopores is advantageous for the exposure of active sites and mass diffusion for catalytic reaction. The BET-specific surface area of the PtNi@GCNs is measured to be 208.5 $m^2\ g^{-1}$. The surface composition of the PtNi@GCNs was examined by XPS. The survey scan spectrum (Figure 5b) corroborates that the PtNi@GCNs are composed by Pt, Ni, and C. The high-resolution Pt 4f spectrum (Figure 5c) indicates that Pt exists predominantly as metallic Pt. The high-resolution Ni 2p spectrum can be well deconvoluted into metallic Ni and oxidized species (Figure 5d). The Ni-based oxidized species might be caused by the surface oxidation of the PtNi@GCNs.

As is well known, nitroaromatics are hazardous pollutants in industrial and agricultural fields, whereas the hydrogenated products of nitroaromatics, aromatic amines, are key intermediates for pharmaceutical and chemical industries.[36−40] The hydrogenation of nitroaromatics catalyzed by a noble metal-based catalyst represents an efficient and eco-friendly strategy to produce aromatic amines.[41−48] Because of the unique 2D architecture and enriched firmly immobilized PtNi NPs, the as-prepared PtNi@GCN sample is reasonably expected to be a high-efficient catalyst with superior activity and high durability. As a proof-of-concept application, the catalytic activity of the PtNi@GCN sample was appraised by the hydrogenation of 4-NP with the assistance of a reducing agent of $NaBH_4$, as illustrated in Figure 6a. The catalytic performance was benchmarked against the commercial Pt/C (20 wt %) catalyst. The stepwise hydrogenation process can be monitored by UV−vis spectroscopy. As shown in Figure 6b, upon the introduction of the PtNi@GCN catalyst, the color of the 4-nitrophenolate solution (caused by the reaction between 4-NP and $NaBH_4$) changes from light yellow to colorless in 8 min, indicating the completion of the hydrogenation reaction. Time-dependent UV absorption spectra indicate that the characteristic absorption peak of 4-nitrophenolate at 405 nm decreases rapidly accompanied by a successive increase at the 302 nm peak assigned to 4-AP. By contrast, it takes 28 min for the commercial Pt/C catalyst to complete the reaction under an identical condition, as evidenced by the UV absorption spectra in Figure S1 of the Supporting Information.

The concentration of $NaBH_4$ considerably exceeds that of 4-NP and thus can be considered as a constant during the entire reaction course. Therefore, the hydrogenation reaction follows the pseudo-first-order kinetics depending on the concentration of 4-NP, and the $\ln(C_t/C_0)$ is linear with the reaction time t, where C_t and C_0 refer to the concentration of 4-NP at t and initial solution, respectively. Figure 6c clearly shows the linear correlationship between $\ln(C_t/C_0)$ and t, and the rate constant (k) of the PtNi@GCN catalyst is calculated to be 0.28 min^{-1}, which is three times higher than that of the commercial Pt/C catalyst (0.09 min^{-1}). The recyclability of a catalyst is also a crucial parameter for practical applications. As suggested by Figure 6d, the PtNi@GCN catalyst could still maintain high activity after five cycles, without evident deactivation during the long-term operation. The TEM image (Figure 6e) indicates that the PtNi NPs are still uniformly dispersed in the carbon sheets, without aggregation or detachment from the carbon support. All these results strongly suggest that the as-prepared PtNi@GCN catalyst is a highly efficient catalyst for hydrogenation of 4-NP with superior activity and high stability. The excellent catalytic performance of the resulting PtNi@GCN catalyst might be attributed to its unique architectural feature and favorable compositions. Specifically, (1) plenty of highly dispersed PtNi NPs could provide a high density of active sites for the hydrogenation reaction; (2) the 2D carbon nanosheets with high conductivity facilitate the electron transfer from donor ($NaBH_4$) to acceptor (nitrophenolate), expediting the hydrogenation reaction; (3) the firm immobilization of PtNi NPs with 2D carbon nanosheets could effectively prevent the detachment or aggregation of active sites during the reaction, thus remarkably increasing their stability.

4. CONCLUSIONS

In summary, we have presented a facile and scalable approach for the fabrication of uniform PtNi NP-embedded 2D graphitic carbon nanosheets by using inexpensive NaCl as a recyclable template. The firm immobilization of PtNi NPs within 2D carbon nanosheets could effectively suppress the detachment or aggregation of PtNi NPs during the catalytic reaction. Thanks to the unique architectural feature and favorable compositions, the prepared PtNi@GCN catalyst is demonstrated to be a catalyst with outstanding activity and robust stability for the hydrogenation of 4-NP, suggesting that the PtNi@GCN catalyst may hold great promise in environmental remediation and so forth. We believe that the present versatile synthetic methodology can be extendable to the rational design of carbon nanosheet-based nanohybrids for diverse applications in the future.

■ ASSOCIATED CONTENT

Supporting Information

The Supporting Information is available free of charge on the ACS Publications website at DOI: 10.1021/acsomega.8b02746.

Time-dependent UV−vis spectra for the catalytic reduction of 4-NP by $NaBH_4$ in the presence of the commercial Pt/C (20 wt %) catalyst (PDF)

■ AUTHOR INFORMATION

Corresponding Authors

*E-mail: xulin001@njnu.edu.cn (L.X.).
*E-mail: jyang@ipe.ac.cn (J.Y.).

DOI: 10.1021/acsomega.8b02746
ACS Omega 2018, 3, 16436−16442

ORCID

Jun Yang: 0000-0002-8993-0655

Notes

The authors declare no competing financial interest.

■ ACKNOWLEDGMENTS

Financial supports from the National Natural Science Foundation of China (grant nos. 21503111, 21573240), Natural Science Foundation of Jiangsu Higher Education Institutions of China (grant no. 16KJB150020), Natural Science Foundation of Jiangsu Province (BK20171473), 2017 Jurong SME Technology Innovation Project (CX2017006), and Center for Mesoscience, Institute of Process Engineering, Chinese Academy of Sciences (grant nos. COM2015A001 and MPCS-2017-A-02) are gratefully acknowledged.

■ REFERENCES

(1) Gao, Y.; Zhang, X.; Li, Y.; Liu, H.; Wang, Y.; Chang, Q.; Jiao, W.; Song, Y. Saturable Absorption and Reverse Saturable Absorption in Platinum Nanoparticles. *Opt. Commun.* **2005**, *251*, 429−433.

(2) Mikhelashvili, V.; Padmanabhan, R.; Meyler, B.; Yofis, S.; Atiya, G.; Cohen-Hyams, Z.; Weindling, S.; Ankonina, G.; Salzman, J.; Kaplan, W. D.; Eisenstein, G. Optically Sensitive Devices Based on Pt Nano Particles Fabricated by Atomic Layer Deposition and Embedded in a Dielectric Stack. *J. Appl. Phys.* **2015**, *118*, 134504.

(3) Kang, T. D.; Yoon, J.-G. Optical Characterization of Surface Plasmon Resonance of Pt Nanoparticles in TiO_2-SiO_2 Nanocomposite Films. *J. Appl. Phys.* **2017**, *122*, 134302.

(4) Wang, W.-N.; An, W.-J.; Ramalingam, B.; Mukherjee, S.; Niedzwiedzki, D. M.; Gangopadhyay, S.; Biswas, P. Size and Structure Matter: Enhanced CO_2 Photoreduction Efficiency by Size-Resolved Ultrafine Pt Nanoparticles on TiO_2 Single Crystals. *J. Am. Chem. Soc.* **2012**, *134*, 11276−11281.

(5) Schweinberger, F. F.; Berr, M. J.; Döblinger, M.; Wolff, C.; Sanwald, K. E.; Crampton, A. S.; Ridge, C. J.; Jäckel, F.; Feldmann, J.; Tschurl, M.; Heiz, U. Cluster Size Effects in the Photocatalytic Hydrogen Evolution Reaction. *J. Am. Chem. Soc.* **2013**, *135*, 13262−13265.

(6) Kalisman, P.; Nakibli, Y.; Amirav, L. Perfect Photo-to-Hydrogen Conversion Efficiency. *Nano Lett.* **2016**, *16*, 1776−1781.

(7) Jin, J.; Wang, C.; Ren, X.-N.; Huang, S.-Z.; Wu, M.; Chen, L.-H.; Hasan, T.; Wang, B.-J.; Li, Y.; Su, B.-L. Anchoring Ultrafine Metallic and Oxidized Pt Nanoclusters on Yolk-Shell TiO_2 for Unprecedentedly High Photocatalytic Hydrogen Production. *Nano Energy* **2017**, *38*, 118−126.

(8) Liang, H.-P.; Zhang, H.-M.; Hu, J.-S.; Guo, Y.-G.; Wan, L.-J.; Bai, C.-L. Pt Hollow Nanospheres: Facile Synthesis and Enhanced Electrocatalysts. *Angew. Chem., Int. Ed.* **2004**, *43*, 1540−1543.

(9) Antolini, E.; Lopes, T.; Gonzalez, E. R. An Overview of Platinum-Based Catalysts as Methanol-Resistant Oxygen Reduction Materials for Direct Methanol Fuel Cells. *J. Alloys Compd.* **2008**, *461*, 253−262.

(10) Chen, A.; Holt-Hindle, P. Platinum-Based Nanostructured Materials: Synthesis, Properties, and Applications. *Chem. Rev.* **2010**, *110*, 3767−3804.

(11) Yang, J.; Ying, J. Y. Nanocomposites of Ag_2S and Noble Metals. *Angew. Chem., Int. Ed.* **2011**, *50*, 4637−4643.

(12) Wang, Y.-J.; Wilkinson, D. P.; Zhang, J. Noncarbon Support Materials for Polymer Electrolyte Membrane Fuel Cell Electrocatalysts. *Chem. Rev.* **2011**, *111*, 7625−7651.

(13) Feng, Y.; Liu, H.; Wang, P.; Ye, F.; Tan, Q.; Yang, J. Enhancing the Electrocatalytic Property of Hollow Structured Platinum Nanoparticles for Methanol Oxidation Through a Hybrid Construction. *Sci. Rep.* **2014**, *4*, 6204.

(14) Wang, Y.-J.; Zhao, N.; Fang, B.; Li, H.; Bi, X. T.; Wang, H. Carbon-Supported Pt-Based Alloy Electrocatalysts for the Oxygen Reduction Reaction in Polymer Electrolyte Membrane Fuel Cells: Particle Size, Shape, and Composition Manipulation and Their Impact to Activity. *Chem. Rev.* **2015**, *115*, 3433−3467.

(15) Cui, P.; He, H.; Liu, H.; Zhang, S.; Yang, J. Heterogeneous Nanocomposites of Silver Selenide and Hollow Platinum Nanoparticles toward Methanol Oxidation Reaction. *J. Power Sources* **2016**, *327*, 432−437.

(16) Shao, M.; Chang, Q.; Dodelet, J.-P.; Chenitz, R. Recent Advances in Electrocatalysts for Oxygen Reduction Reaction. *Chem. Rev.* **2016**, *116*, 3594−3657.

(17) Feng, Y.; Liu, H.; Yang, J. A Selective Electrocatalyst-Based Direct Methanol Fuel Cell Operated at High Concentration of Methanol. *Sci. Adv.* **2017**, *3*, e1700580.

(18) Tang, J.; Chen, D.; Yao, Q.; Xie, J.; Yang, J. Recent Advances in Noble Metal-Based Nanocomposites for Electrochemical Reactions. *Mater. Today Energy* **2017**, *6*, 115−127.

(19) Zhang, C.; Liu, F.; Zhai, Y.; Ariga, H.; Yi, N.; Liu, Y.; Asakura, K.; Flytzani-Stephanopoulos, M.; He, H. Alkali-Metal-Promoted Pt/TiO_2 Opens a More Efficient Pathway to Formaldehyde Oxidation at Ambient Temperatures. *Angew. Chem., Int. Ed.* **2012**, *51*, 9628−9632.

(20) Huang, H.; Hu, P.; Huang, H.; Chen, J.; Ye, X.; Leung, D. Y. C. Highly Dispersed and Active Supported Pt Nanoparticles for Gaseous Formaldehyde Oxidation: Influence of Particle Size. *Chem. Eng. J.* **2014**, *252*, 320−326.

(21) Qi, L.; Cheng, B.; Ho, W.; Liu, G.; Yu, J. Hierarchical Pt/NiO Hollow Microspheres with Enhanced Catalytic Performance. *ChemNanoMat* **2015**, *1*, 58−67.

(22) Chen, H.; Tang, M.; Rui, Z.; Ji, H. MnO_2 Promoted TiO_2 Nanoplate Array Supported Pt Catalyst for Formaldehyde Oxidation with Enhanced Efficiency. *Ind. Eng. Chem. Res.* **2015**, *54*, 8900−8907.

(23) Li, J.; Tang, W.; Liu, G.; Li, W.; Deng, Y.; Yang, J.; Chen, Y. Reduced Graphene Oxide Modified Platinum Catalysts for the Oxidation of Volatile Organic Compounds. *Catal. Today* **2016**, *278*, 203−208.

(24) Li, J.; Feng, Y.; Mo, S.; Liu, H.; Chen, Y.; Yang, J. Nanodendritic Platinum Supported on γ-Alumina for Complete Benzene Oxidation. *Part. Part. Syst. Charact.* **2016**, *33*, 620−627.

(25) Li, J.; Liu, H.; Deng, Y.; Liu, G.; Chen, Y.; Yang, J. Emerging Nanostructured Materials for the Catalytic Removal of Volatile Organic Compounds. *Nanotechnol. Rev.* **2016**, *5*, 147−181.

(26) Liu, H.; Li, C.; Ren, X.; Liu, K.; Yang, J. Fine Platinum Nanoparticles Supported on a Porous Ceramic Membrane as Efficient Catalysts for the Removal of Benzene. *Sci. Rep.* **2017**, *7*, 16589.

(27) Shang, L.; Bian, T.; Zhang, B.; Zhang, D.; Wu, L.-Z.; Tung, C.-H.; Yin, Y.; Zhang, T. Graphene-Supported Ultrafine Metal Nanoparticles Encapsulated by Mesoporous Silica: Robust Catalysts for Oxidation and Reduction Reactions. *Angew. Chem., Int. Ed.* **2014**, *53*, 250−254.

(28) Huang, W.; Wang, H.; Zhou, J.; Wang, J.; Duchesne, P. N.; Muir, D.; Zhang, P.; Han, N.; Zhao, F.; Zeng, M. Highly Active and Durable Methanol Oxidation Electrocatalyst Based on the Synergy of Platinum-Nickel Hydroxide-Graphene. *Nat. Commun.* **2015**, *6*, 10035.

(29) Zhan, G.; Zeng, H. C. General Strategy for Preparation of Carbon-Nanotube-Supported Nanocatalysts with Hollow Cavities and Mesoporous Shells. *Chem. Mater.* **2015**, *27*, 726−734.

(30) Guo, S.; Dong, S.; Wang, E. Three-Dimensional Pt-on-Pd Bimetallic Nanodendrites Supported on Graphene Nanosheet: Facile Synthesis and Used as an Advanced Nanoelectrocatalyst for Methanol Oxidation. *ACS Nano* **2009**, *4*, 547−555.

(31) Wang, R.; Wu, Z.; Chen, C.; Qin, Z.; Zhu, H.; Wang, G.; Wang, H.; Wu, C.; Dong, W.; Fan, W.; Wang, J. Graphene-Supported Au−Pd Bimetallic Nanoparticles with Excellent Catalytic Performance in Selective Oxidation of Methanol to Methyl Formate. *Chem. Commun.* **2013**, *49*, 8250−8252.

(32) Wang, H.; Yan, X.; Huang, Y.; Zhang, M.; Tang, Y.; Sun, D.; Xu, L.; Wei, S. Cyanogel-Derived N-Doped C Nanosheets Immobilizing Pd-P Nanoparticles: One-Pot Synthesis and Enhanced Hydrogenation Catalytic Performance. *Appl. Surf. Sci.* **2017**, *396*, 812−820.

(33) Zhou, G.; Yang, Q.; Guo, X.; Chen, Y.; Yang, Q.; Xu, L.; Sun, D.; Tang, Y. Coupling Molybdenum Carbide Nanoparticles with N-Doped

DOI: 10.1021/acsomega.8b02746
ACS Omega 2018, 3, 16436−16442

Carbon Nanosheets as a High-Efficiency Electrocatalyst for Hydrogen Evolution Reaction. *Int. J. Hydrogen Energy* **2018**, *43*, 9326−9333.
(34) Zhang, J.; Zhu, H.; Wu, P.; Ge, C.; Sun, D.; Xu, L.; Tang, Y.; Zhou, Y. Rational Synthesis of Ni Nanoparticle-Embedded Porous Graphitic Carbon Nanosheets with Enhanced Lithium Storage Properties. *Nanoscale* **2015**, *7*, 18211−18217.
(35) Fan, C.; Huang, Z.; Hu, X.; Shi, Z.; Shen, T.; Tang, Y.; Wang, X.; Xu, L. Freestanding Pt Nanosheets with High Porosity and Improved Electrocatalytic Performance toward the Oxygen Reduction Reaction. *Green Energy Environ.* **2018**, *3*, 310−317.
(36) Keith, L.; Telliard, W. ES&T Special Report: Priority Pollutants: I-A Perspective View. *Environ. Sci. Technol.* **1979**, *13*, 416−423.
(37) Ju, K.-S.; Parales, R. E. Nitroaromatic Compounds, from Synthesis to Biodegradation. *Microbiol. Mol. Biol. Rev.* **2010**, *74*, 250−272.
(38) Franck, H. G.; Stadelhofer, J. W. *Industrial Aromatic Chemistry: Raw Materials Processes Products*; Springer Science & Business Media, 2012.
(39) Yun, H.; Liang, B.; Kong, D.-Y.; Cheng, H.-Y.; Li, Z.-L.; Gu, Y.-B.; Yin, H.-Q.; Wang, A.-J. Polarity Inversion of Bioanode for Biocathodic Reduction of Aromatic Pollutants. *J. Hazard. Mater.* **2017**, *331*, 280−288.
(40) Zhang, L.; Niu, C.-G.; Wen, X.-J.; Guo, H.; Zhao, X.-F.; Liang, C.; Zeng, G.-M. Enhanced Photocatalytic Activity of CdS/SnS_2 Nanocomposite with Highly-Efficient Charge Transfer and Visible Light Utilization for Selective Reduction of 4-Nitroaniline. *J. Colloid Interface Sci.* **2018**, *532*, 557−570.
(41) An, Q.; Yu, M.; Zhang, Y.; Ma, W.; Guo, J.; Wang, C. Fe_3O_4@Carbon Microsphere Supported Ag−Au Bimetallic Nanocrystals with the Enhanced Catalytic Activity and Selectivity for the Reduction of Nitroaromatic Compounds. *J. Phys. Chem. C* **2012**, *116*, 22432−22440.
(42) Yang, M.-Q.; Pan, X.; Zhang, N.; Xu, Y.-J. A Facile One-Step Way to Anchor Noble Metal (Au, Ag, Pd) Nanoparticles on a Reduced Graphene Oxide Mat with Catalytic Activity for Selective Reduction of Nitroaromatic Compounds. *CrystEngComm* **2013**, *15*, 6819−6828.
(43) Lu, Y.-M.; Zhu, H.-Z.; Li, W.-G.; Hu, B.; Yu, S.-H. Size-Controllable Palladium Nanoparticles Immobilized on Carbon Nanospheres for Nitroaromatic Hydrogenation. *J. Mater. Chem. A* **2013**, *1*, 3783−3788.
(44) Tuo, Y.; Liu, G.; Dong, B.; Zhou, J.; Wang, A.; Wang, J.; Jim, R.; Lv, H.; Dou, Z.; Huang, W. Microbial Synthesis of Pd/Fe_3O_4, Au/Fe_3O_4 and PdAu/Fe_3O_4 Nanocomposites for Catalytic Reduction of Nitroaromatic Compounds. *Sci. Rep.* **2015**, *5*, 13515.
(45) Zhao, Y.; Luo, Y.; Yang, X.; Yang, Y.; Song, Q. Tunable Preparation of Ruthenium Nanoparticles with Superior Size-Dependent Catalytic Hydrogenation Properties. *J. Hazard. Mater.* **2017**, *332*, 124−131.
(46) Wang, S.; Fu, J.; Wang, K.; Gao, M.; Wang, X.; Wang, Z.; Chen, J.; Xu, Q. Facile Synthesis of Pd Nanoparticles on Polydopamine-Coated Fe-Fe_2O_3 Magnetic Nanochains as Recyclable High-Performance Nanocatalysts. *Appl. Surf. Sci.* **2018**, *459*, 208−216.
(47) Zhang, Q.; Jin, X.; Xu, Z.; Zhang, J.; Rendón, U. F.; Razzari, L.; Chaker, M.; Ma, D. Plasmonic Au-Loaded Hierarchical Hollow Porous TiO_2 Spheres: Synergistic Catalysts for Nitroaromatic Reduction. *J. Phys. Chem. Lett.* **2018**, *9*, 5317−5326.
(48) Millán, R.; Liu, L.; Boronat, M.; Corma, A. A New Molecular Pathway Allows the Chemoselective Reduction of Nitroaromatics on Non-Noble Metal Catalysts. *J. Catal.* **2018**, *364*, 19−30.

DOI: 10.1021/acsomega.8b02746
ACS Omega 2018, 3, 16436−16442